Supplementary information

Mechanical Degradation of Polyacrylamide at Ultra High Deformation Rates during Hydraulic Fracturing

Boya Xiong[1], Prakash Purswani[4], Taylor Pawlik[3], Laxmicharan Samineni[3], Zuleima T. Karpyn[4], Andrew L. Zydney[3], Manish Kumar[2,3]

[1]Department of Civil and Environmental Engineering; Massachusetts Institute of Technology; [2]Department of Civil and Environmental Engineering; [3]Department of Chemical Engineering; [4]John and Willie Leone Family Department of Energy and Mineral Engineering; The Pennsylvania State University

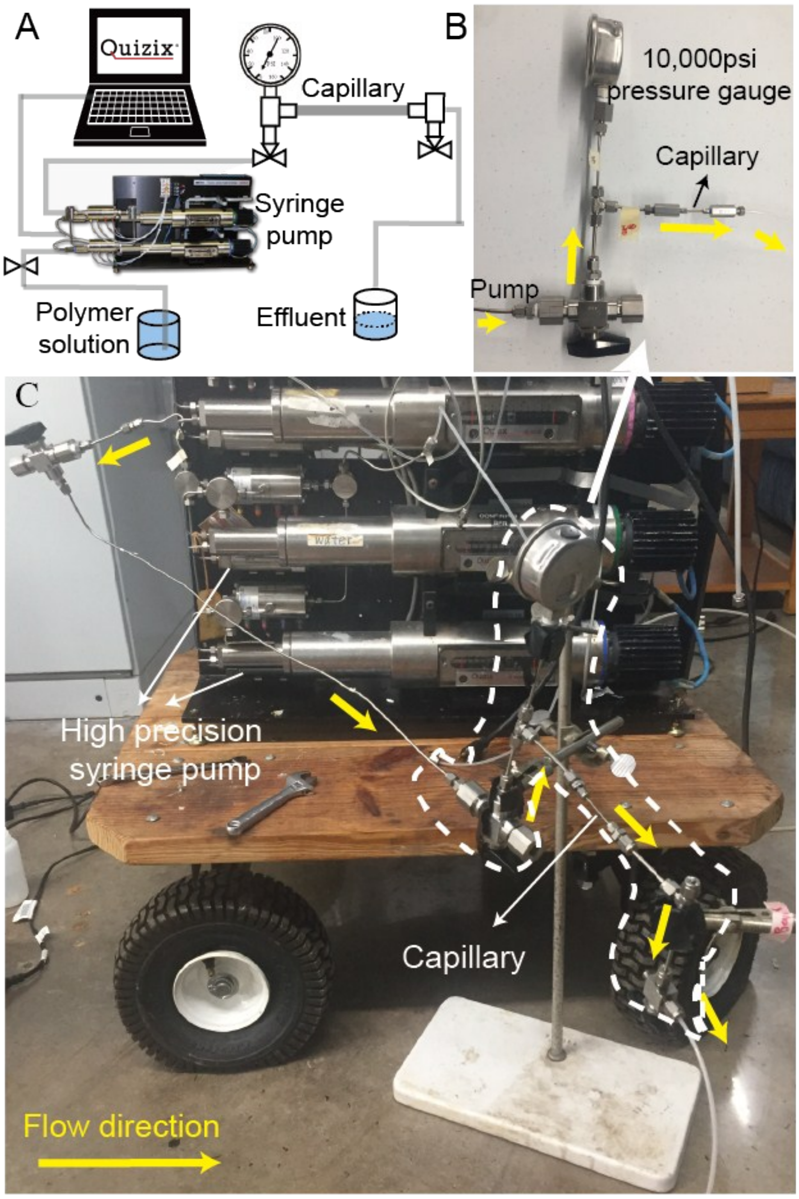

Figure S1. (A): Schematic, (B) and (C): Images of the capillary flow set up.

Shear rate calculation

The shear stress (τ) and viscosity (η) of a power law fluid, such as a polyacrylamide solution, are a function of the shear rate (γ), which is often represented by a simple power law expression:

$$\tau = \eta\gamma = K\gamma^n \qquad [1]$$

where K is a consistency factor and n is the power law index; these values depend on the molecular weight and concentration of the polymer. Previous studies have shown that polyacrylamide solutions behave as Newtonian fluids at low shear rate (n=1), and as shear thinning fluids (pseudoplastic, n<1) at increased shear rates up until a critical shear rate (γ_c), and become shear thickening shortly (dilatant, n>1) then transit back to Newtonian fluids regime at higher shear rates.

The momentum conservation equations for flow in a tube give the following relationship between the pressure drop and shear stress for a power-law fluid:

$$-\Delta P = 2\frac{L}{r}\tau = 2\frac{L}{r}K\left(\frac{du}{dr}\right)^n \qquad [2]$$

where r is the radial position and L is the tube length. Eq. (2) can be integrated over r, with a no-slip boundary condition (u=0) applied at the tube radius (r=R), to obtain the velocity profile and the following relationship between the pressure drop and the bulk average velocity:

$$u = -\left(-\frac{1\Delta P}{2KL}\right)^{\frac{1}{n}}\left(\frac{n}{n+1}\right)\left(R^{\left(\frac{n+1}{n}\right)} - r^{\left(\frac{n+1}{n}\right)}\right) \qquad [3]$$

$$\Delta P = \frac{2\left(\frac{3n+1}{n}\right)^n LKV^n}{R^{n+1}}$$

[4]

$$\log \Delta P = \log\left[\frac{2\left(\frac{3n+1}{n}\right)^n LK}{R^{n+1}}\right] + n\log V \qquad [5]$$

The best fit values of n and K were determined based on a log-log plot of ΔP as a function of V (Table S1) using Eq. (5), with the shear rate and strain rate then calculated using **Eqn S6 and S7[1].**

$\dot{\gamma}_v = \left(\frac{3n+1}{n}\right)\frac{V}{R}$ (Velocity derived, the derivative product of equation 3 over r with boundary conditions stated above) [6]

$\dot{\gamma}_p = \left(\frac{\Delta Pr}{2LK}\right)^{1/n}$ (Pressure derived, re-arranged from equation 2) [7]

$$\dot{\gamma}_w = \frac{\Delta P r}{8\eta L}$$ (Wall shear rate, η is solvent viscosity)[2] [8]

$$\dot{\varepsilon} = 0.56\frac{V}{R}$$ (characteristic strain rate)[3] [9]

Table S1. A example calculation of n, K, and shear rate value ($\dot{\gamma}$) using pressure and flow rate data from experiments using 75 µm capillary. Averaging six groups of n and K values yielded from triplicated flow experiments with 50 and 75 µm capillary indicates a n value of 1.001 ± 0.025 and a K value of 0.00116 ± 0.000047.

P ($kg \cdot m^{-1} \cdot s^{-2}$)	V (m/s)	Log P	Log V	n	K (Pa · s)	$\dot{\gamma}$ (s^{-1})	$\dot{\varepsilon}$ (s^{-1})	$\frac{V}{R}$ (s^{-1})
7.7×10^5	2	5.89	0.28	0.9734	2.1×10^{-3}	2.03×10^{5}	2.82×10^{4}	5.03×10^{4}
1.8×10^6	4	6.25	0.58			4.05×10^{6}	5.63×10^{4}	1.01×10^{5}
4.6×10^6	11	6.66	1.05			1.22×10^{6}	1.69×10^{5}	3.02×10^{5}
7.4 10^6	19	6.87	1.28			2.03×10^{6}	2.82×10^{5}	5.03×10^{5}
1.3×10^7	30	7.11	1.48			3.24×10^{6}	4.51×10^{5}	8.05×10^{5}
1.5×10^7	38	7.17	1.58			4.05×10^{6}	5.63×10^{5}	1.01×10^{5}
1.8×10^7	45	7.25	1.66			4.86×10^{6}	6.76×10^{5}	1.21×10^{5}
2.3×10^7	57	7.36	1.75			6.08×10^{6}	8.45×10^{5}	3.02×10^{5}

Estimation of shear rates during hydraulic fracturing operations

During HVHF operations, fracturing fluid is injected at a constant flow rate, passing through perforation holes and flowing into an isolated wellbore space, with the wellbore pressure fluctuating in response to the mechanics of fracture initiation and propagation. Injection pressure (wellbore or bottom-hole pressure) will first increase sharply as a result of fluid compression against the reservoir until the pressure overcomes the reservoir stress and rock tensile strength, initiating fracture formation. At this "breakdown" point, the wellbore pressure relaxes and starts to decrease quickly due to fracture growth. The wellbore pressure then attains a plateau in which the fluid pressure is balanced by the pressure along the fracture and at the fracture tip. After pumping stops (shut-in), fractures start to close and the wellbore pressure decreases more slowly to a value that is close to the reservoir minimal horizontal stress (or closure pressure)[4].

Among the fluid flow events described above, we identified two events that will induce very high shear rates: flow through perforations and flow into initial fractures during fracture propagation. We estimated the shear rates in these two situations based on the net pressure, which is roughly the difference between the fluid injection pressure (after accounting for frictional loss) and the minimal horizontal in-situ stress. Perforating wellbores create 0.005-0.02 m size holes[5-7] with penetrating depths of 0.2-1.0 m into the formation[5]. The perforation holes were modeled as cylinders while the fracture geometry was assumed to be a thin rectangular plane based on the commonly accepted 2D fracture geometry feature of the Perkins-Kern-Nordgren (PKN) model[8]. The fracture is assumed to grow with a constant height (h_f) with the growing half-length (X_f) being much longer than h_f, and a width (w) ranging from 0.5-5 mm[6, 9-13]. The maximum shear rate within the rectangular fracture for a power law fluid was evaluated as[14]:

$$\dot{\gamma}_f = \left(\frac{h_f \Delta P}{2X_f K(\frac{h_f}{W}+1)}\right)^{1/n} \qquad [10]$$

The injection and wellbore pressures can be estimated based on formation depth (1000-10,000 psi[15]), but the net pressure (ΔP) is still highly uncertain given the difficulty in estimating the in-situ horizontal stress (3000-9000 psi[4, 7, 12, 16]) as well as the fracture and formation properties. Thus, ΔP both prior to and during breakdown was assumed to be 200-2000 psi[4, 7, 11, 16, 17] (roughly the wellbore pressure minus the horizontal stress). We also considered the pressure loss due to frictional flow in the wellbore ($P_{wellbore}$) and through the perforations ($P_{perofration}$)[7]:

$$P_{perforation} = \frac{0.807\, Q_p^2 \rho_s}{{N_p}^2 {d_p}^4 {K_d}^2} \qquad [11]$$

where Q_p is the injection rate in each perforation, ρ_s is the fluid density, N_p is the number of perforations, d_p is the perforation diameter, and K_d is a dimensionless discharge coefficient ($K_d \approx 0.75$) and

$$P_{wellbore} = 2^{3n+2} \pi^{-n} K \left(\frac{1+3n}{n}\right)^n D^{-(3n+1)} Q \qquad [12]$$

where Q is the total injection rate and D is the wellbore diameter. This calculation suggests these frictional losses (1~100 psi) are relatively small compared to the total net injection pressure[7]. The following assumptions were made to simplify the calculations (**Table S3**):

1. There were no pre-existing fractures in the formation or fluid loss due to poor casing.
2. Each perforation-cluster successfully yields one major developed fracture[11, 17, 18]. Other branching fractures surrounding the main fracture are neglected[17]..
3. The number of perforation in each cluster (N_p) is equal to the average number of perforation per foot[5] multiplied by the length of one cluster[19], giving $N_p = 16$.
4. Fractures vertically to the wellbore, neglecting the surface roughness, shape irregularity, and side fractures.
5. The power law parameters were n=0.97 and K=2.1 × 10^{-3}.

Table S2. Operational specifics for one single stage hydraulic fracturing operation.

	Operational specifics	**Range in literature**	**Midrange Value**
Stage	Stage length (m)	30-180[19]	107
	Fracture spacing (m)	12-120[7, 11, 16-18]	98
	Number of clusters or fractures (N_f)	N/A	1
	Wellbore diameter (D, m)		0.1[7]
	Injection rate (Q, m^3/s)	0.05-0.24[6, 7, 11, 20]	0.14
	Wellbore pressure (psi)	1000-10,000[15]	
	Net pressure (psi)	200-2000[4]	
Perforation	Number of perforation per meter	13-40[5, 11]	26
	Length of one cluster (m)	0.6[19]	0.6
	Number of perforation (N_p)		16
	Perforation diameter (d_p, m)	0.005-0.02[5-7]	
	Perforation length (m)	0.21-1[5]	0.6
Propagating fracture	Fracture width (W, m)	0.005-0.0005[6, 9-13]	0.0027
	Fracture half length (X_f, m)	90-220[11, 13, 16, 17]	
	Developed fracture height (h_f, m)	15-121[11, 13, 16, 17]	68

Table S3. Geometry, dimension range, and equations for calculating the shear rate during flow through perforations and propagating fractures for a given perforation diameter (d_p) and fracture half-length (X_f). Net pressures of 200 and 3000 psi were used as the low and high pressure drops in the fracture.
.

	Perforation			**Propagating fracture**		
Geometry	Cylinder			Rectangular plane (modified PKN model[8])		
Dimension (m)	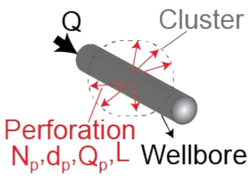 d_p: 0.005-0.02 L=0.6			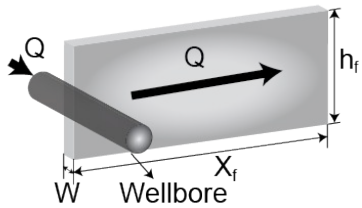 W=0.00275; h_f=68 X_f=0.1-220		
Shear rate equation (s^{-1})	$\dot{\gamma}_p = (\frac{\Delta P r}{2LK})^{1/n}$			$\dot{\gamma}_f = (\frac{h_f \Delta P}{2X_f K(\frac{h_f}{W}+1)})^{1/n}$		
	d_p(m)	$\dot{\gamma}_p$ (max, s^{-1}, ΔP=2000 psi)	$\dot{\gamma}_p$ (min, s^{-1}, ΔP=200 psi)	X_f (m)	$\dot{\gamma}_f$ (max, s^{-1}, ΔP=2000 psi)	$\dot{\gamma}_f$ (min, s^{-1}, ΔP=200 psi)
	0.02	1.1×10^8	7.0×10^6	0.1	8.4×10^7	1.3×10^6
	0.01	5.2×10^7	3.4×10^6	20	4.2×10^5	1.3×10^4
	0.008	4.2×10^7	2.6×10^6	100	8.5×10^5	2.6×10^3
	0.005	2.5×10^7	7.8×10^5	220	3.9×10^4	1.2×10^3
Shear rate range (s^{-1})	10^5-10^8			10^3-10^7		

Reference:

1. Nguyen, T. Q.; Kausch, H.-H., Chain extension and degradation in convergent flow. *Polymer* **1992,** *33*, (12), 2611-2621.

2. Vanapalli, S. A.; Islam, M. T.; Solomon, M. J., Scission-induced bounds on maximum polymer drag reduction in turbulent flow. *Phys. Fluids* **2005,** *17*, (9), 095108.

3. Metzner, A. B.; Metzner, A. P., Stress levels in rapid extensional flows of polymeric fluids. *Rheol. Acta.* **1970,** *9*, (2), 174-181.

4. Montgomery, M. B. S. a. C. T., Hydraulic fracturing In Dandekar, A. Y., Ed. CRC Press
Taylor & Francis Group: 2015.

5. Hansen, B., Casing perforating overview. *URL:* http://water. *epa. gov/type/groundwater/uic/class2/hydraulicfracturing/upload/casingperforatedoverview. pdf (visited on 06/01/2015)* **2015**.

6. Geertsma, J.; De Klerk, F., A rapid method of predicting width and extent of hydraulically induced fractures. *Journal of Petroleum Technology* **1969,** *21*, (12), 1,571-1,581.

7. Wu, K.; Olson, J. E., Mechanisms of simultaneous hydraulic-fracture propagation from multiple perforation clusters in horizontal wells. *SPE Journal* **2016,** *21*, (03), 1,000-1,008.

8. Perkins, T.; Kern, L., Widths of hydraulic fractures. *Journal of Petroleum Technology* **1961,** *13*, (09), 937-949.

9. Lin, C.; He, J.; Li, X., Width evolution of the hydraulic fractures in different reservoir rocks. *Rock Mechanics and Rock Engineering* **2018**, 1-7.

10. Britt, L., Fracture stimulation fundamentals. *Journal of Natural Gas Science and Engineering* **2012,** *8*, 34-51.

11. Zeng, F.; Guo, J., Optimized design and use of induced complex fractures in horizontal wellbores of tight gas reservoirs. *Rock Mechanics and Rock Engineering* **2016,** *49*, (4), 1411-1423.

12. Roussel, N. P.; Sharma, M. M., Optimizing fracture spacing and sequencing in horizontal-well fracturing. *SPE Production & Operations* **2011,** *26*, (02), 173-184.

13. Cheng, Y. In *Boundary element analysis of the stress distribution around multiple fractures: Implications for the spacing of perforation clusters of*

hydraulically fractured horizontal wells, SPE Eastern Regional Meeting, 2009; Society of Petroleum Engineers: 2009.

14. Son, Y., Determination of shear viscosity and shear rate from pressure drop and flow rate relationship in a rectangular channel. *Polymer* **2007,** *48*, (2), 632-637.

15. Sumner, A. J.; Plata, D. L., Exploring the hydraulic fracturing parameter space: A novel high-pressure, high-throughput reactor system for investigating subsurface chemical transformations. *Environ. Sci. Process Impacts* **2018,** *20*, (2), 318-331.

16. Roussel, N. P.; Manchanda, R.; Sharma, M. M. In *Implications of fracturing pressure data recorded during a horizontal completion on stage spacing design*, SPE Hydraulic Fracturing Technology Conference, 2012; Society of Petroleum Engineers: 2012.

17. Cheng, Y., Impacts of the number of perforation clusters and cluster spacing on production performance of horizontal shale-gas wells. *SPE Reservoir Evaluation & Engineering* **2012,** *15*, (01), 31-40.

18. Ren, L.; Lin, R.; Zhao, J.; Wu, L., An optimal design of cluster spacing intervals for staged fracturing in horizontal shale gas wells based on the optimal srvs. *Natural Gas Industry B* **2017,** *4*, (5), 364-373.

19. Luo, G.; Tian, Y.; Bychina, M.; Ehlig-Economides, C. In *Production optimization using machine learning in bakken shale (just accepted)*, Unconventional Resources Technology Conference, 2018; Society of Exploration Geophysicists, American Association of Petroleum Geologists, Society of Petroleum Engineers: 2018.

20. Wang, Y.; Li, X.; Tang, C., Effect of injection rate on hydraulic fracturing in naturally fractured shale formations: A numerical study. *Environmental Earth Sciences* **2016,** *75*, (11), 935.